ENGLISH VERSION………

Fatigue vulnerability assessment of a steel arch bridge using the probabilistic weibull model and considering its remaining service life under localized corrosion effects

Evaluación de vulnerabilidad a fatiga de un puente de arco en acero, usando el modelo de probabilidad de weibull, considerando la vida remanente en servicio bajo efectos locales de corrosión

Federico Alejandro Núñez Moreno [*1] *https://orcid.org/0000-0002-6011-6553, Luisa Fernanda Lozano Acosta ,[*] María Camila Silva Fajardo [*],
Edgar Eduardo Muñoz Díaz[*], Indira Campo Neira [*]*

* Pontificia Universidad Javeriana., Bogotá – COLOMBIA

Abstract

This study attempts to obtain the approximate fatigue vulnerability of a steel arch bridge from the Colombian national road network. It establishes the interaction between the demand and the available capacity through the Weibull probability equation, and an AASHTO remaining-time equation indicated in (FHWA, 2015). However, the available capacity in terms of the S-N curve obtained from available international references was modified to account for the effects of corrosion present in elements and/or joints in the bridge. The load demand was modeled as the controlled action of the fatigue truck reported in AASHTO, which was systematically located on a structural model represented by Shell and Frame type finite elements, which represented the information available in drawings (in the current Colombian bridge management system), and the one obtained from structural survey activities. The structural model was further calibrated by a parametric study on the modulus of elasticity of steel, which included the minimization of the error difference in the vertical deflections of a bridge load test, keeping the magnitude within the expected ranges established in a protocol. Such reports of actual deflections were achieved using distance meters at important points of the bridge. This model allowed for estimating the magnitude of stresses in the structural elements of the bridge, especially in an area of interest for the study where chemical and physical elements of structural deficiency were determined. The results show an inverse relationship between the probability of failure and remaining service life. The effect of corrosion on the remaining capacity and the probability of failure of the structural elements is clear
.
Keywords: *Fatigue; steel bridges; corrosion effects; cumulative fatigue failure; calibration; progressive collapse.*

Resumen

El presente estudio busca obtener la vulnerabilidad aproximada a fatiga de un Puente de acero en arco que pertenece a la red de vías nacionales de Colombia. Se establece la interacción entre la demanda y la capacidad disponible de resistencia através de la ecuación de probabilidad de Weibull y la ecuación indicada en ela norma AASHTO para vida remanente en fatiga (FHWA, 2015). Sin embargo, la capacidad disponible con base en las curvas S-N de capacidad disponible, se modificaron para poder tener en cuenta los efectos de corrosión presentes en elementos y/o conexiones del puente. La carga se modeló mediante el camion de fatiga especificado en la AASHTO, el cual fue localizado de manera sistemática sobre los nudos de un modelo hecho en elementos finitos tipo Shell and Frame. Este modelo se construyó basado en planos disponibles y de algunas actividades de levantamiento estructural en campo. El modelo estructural fue calibrado mediante un proceso paramétrico en el modulo de elasticidad del acero, el cual minimizó el error entre las deflexiones verticals modealdas y las determinadas mediante una prueba de carga sobre el puente real. Las deflexiones reales fueron reportadas mediane el uso de distanciómetros localizados en puntos seleccionados del puente. El modelo calibrado sirvió para estimar la magbitud de los randos de esfuerzo en los elementos modelados del Puente, especialmente en la zona de estudio, donde se determinó la presencia de corrosión. Los resultados presentan una relación inversa entre la probabilidad de falla por fatiga, y la vida remanente estimada por efectos de fatiga. Se pudo determinar con claridad el efecto de la corrosión en la capacidad del puente y la probabilidad de falla asociada.

Palabras clave: *Fatiga; puentes de acero; efectos de corrosión; falla acumulativa en fatiga; calibración; colapso progresivo.*

¹ Corresponding author:
Pontificia Universidad Javeriana., Bogotá – COLOMBIA
Corresponding author: fnunez@javeriana.edu.co

ENGLISH VERSION………………...

1 Description of Unete Bridge (Casanare - Colombia)

The following is the general methodology used to determine the fatigue vulnerability of a steel arch bridge. The Unete Bridge is in the road corridor between Pajarito and Aguazul in the department of Casanare (Colombia), National Route 62. The structure corresponds to a steel arch bridge, with an underpass, which has a total length of 100m, with two traffic lanes (each lane one-way). The construction date is 2009, which means that, as of 2022, this bridge has a total of 15 years of continuous operation (see Figure 1). According to station 134, which corresponds to road code No 6211, as of 2017, the average daily traffic ADT (average of the last 24 years) of this road corridor is 994 vehicles, with 47% corresponding to heavy traffic, which makes the ADT of trucks 467. It is assumed that this is the dominant condition of traffic over the bridge.

Figure 1. Unete bridge front picture and aerial view using a drone

2. Structural details and materials

The structure is an arched steel bridge, made of ASTM A-588 Gr B steel plates with a yield stress $Fy = 50ksi$ (350MPa), COR-TEN type, which means that the steel-base alloy is resistant to corrosion phenomena by having an integral oxidation control (alloy rich in chromium, manganese, and/or nickel). The bolts used in all the mechanical joint areas correspond to SAE Gr 5 galvanized steel or ASTM A-588. Weldments used an E-90XX electrode, with $Fu=90ksi$ (630MPa). The arch was built with hollow sections including internal stiffeners. The primary girder, which connects the hangers supporting the arch, is a 1/2" (12.7mm) plate girder (See Figure 2).
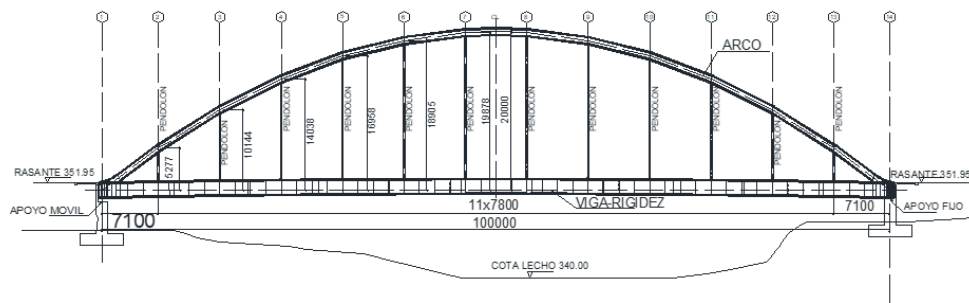

Figure 2. Longitudinal details of the Unete Steel arch bridge

The arch and the girders are braced by two types of bracing systems: i) a nodal bracing system using W-type beams, perpendicular between upstream and downstream elements, and ii) a relative bracing system, made of longitudinally welded L-type shape sections. Above the bracing system of the primary beams, there is a reinforced concrete slab f'c=4,000psi (28MPa) of about 15cm in thickness, with a connection system near the upper flanges of the longitudinal beams of the deck, connected by a system of shear connectors (See Figure 3).
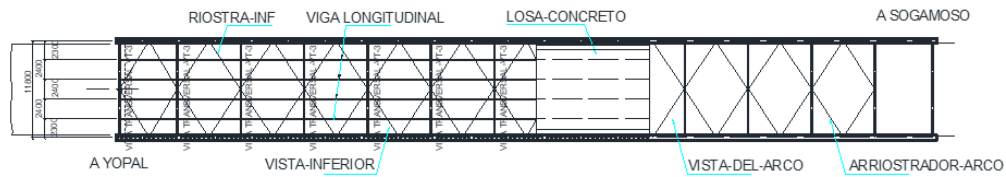
Figure 3. *Unete arch Steel bridge top view of decking system, and arch relative bracing system*

Hangers are elements that theoretically support axial compressive loads, which have a hollow square cross-section. These elements do not function in the same way as cables since, despite being very slender elements, they can resist compressive loads. However, the actual compressive capacity of such a slender element is irrelevant. This hanger is connected using a double perforated plate system, welded to the upper flange of the high web beam with a solid steel pin. The beams of the deck system are connected to the main load-bearing crossed beams (the beams that receive the hangers) using a system of shear connectors with a double line of bolts. The hanger and the main longitudinal beams connection to the deck are classified as critical-fracture elements (FHWA, 2013)

3. Theoretical capacity curves of structural elements vulnerable to fatigue

The typical fatigue resistance curve, also known as the S-N curve, can be obtained for each of the most demanding and important structural elements of the bridge. This can be done by referring to available reference codes (AASHTO, 2017), (JTG-D64, 2015) or by consulting experimental fatigue curves for selected structural elements. According to previous work based on real laboratory data (Ang and Munse, 1975), it is possible to adapt these results to various connection systems in steel bridges, provided that the typologies are similar.

A major step is the identification of the structural categories studied earlier (Ang and Munse, 1975), which can be applied to each element considered as part of the structural model of the bridge under study. Although several categories apply to a structural element, there is always one that generates the lowest remaining fatigue life. That is, there is a category that governs the analysis. For the Unete bridge and the most important structural elements, the categories identified as critical, are available in (Figure 4). The curves (S-N) that were modeled for each structural detail are presented in (Figure 5).
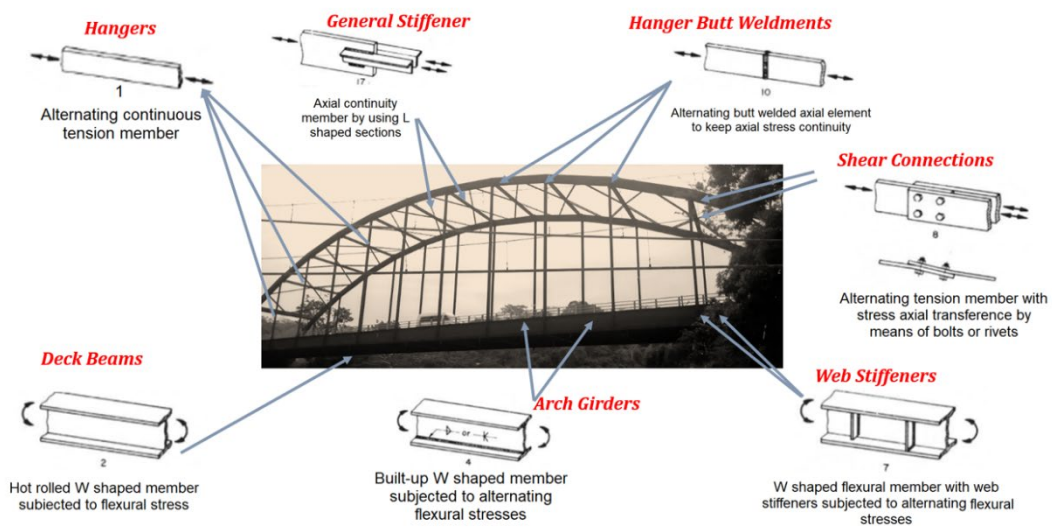

Figure 4. *Structural details identified for the Unete steel arch bridge subjected to fatigue, according to Ang & Munse. Categories identified are 1, 2, 7, 8, 10 and 17. (Ang and Munse, 1975)*

Despite the inherent atmospheric resistance of the steel type used, certain structural elements of the bridge have been subjected to oxidation/corrosion phenomena throughout its service life, as it spans across a river. Therefore, it is crucial to consider the impact of this phenomenon on the nominal fatigue resistance S-N curve. To this end, affecting the slopes of the logarithmic behavior of a reference fatigue

34

capacity curve helps in this task, based on controlled reference tests (Adasooriya et al., 2019a). It was important to make a visual inspection of the structure to determine the areas most affected by such a phenomenon. Although the steel of the structural elements is COR-TEN type, there is evidence of advanced damage in some places near the connections (See (Figure 6)).
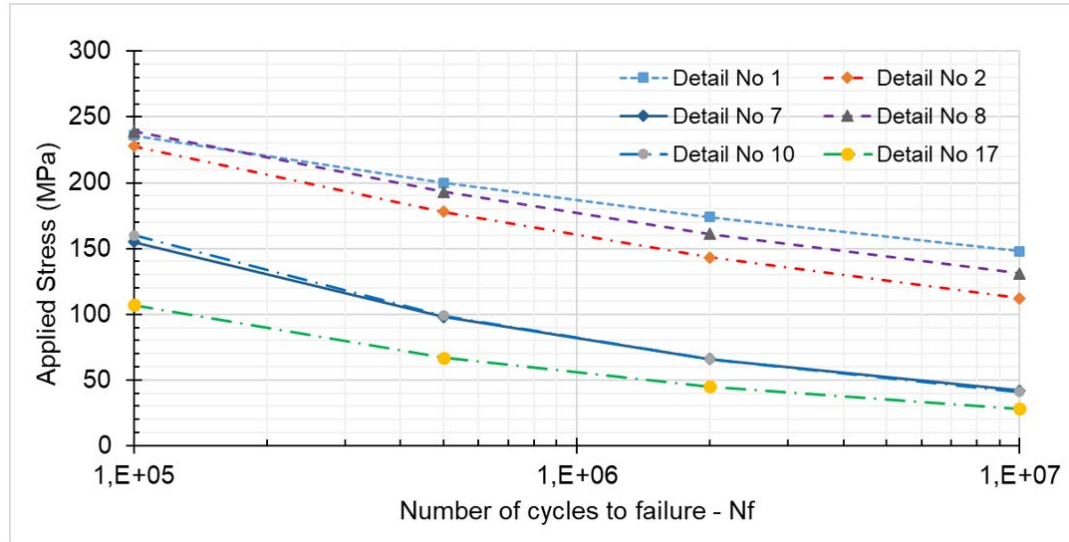

Figure 5. *Fatigue S-N curves for uncorroded Steel for the structural elements fatigue details according to the reported data of (Ang and Munse, 1975)*

As a result of the visual inspection, areas with oxidation and corrosion became clear in one of the structural elements of the bridge, in particular, the main longitudinal arch girder. The visual inspection further confirmed the presence of damage in some structural elements due to possible overloading (localized buckling), as well as the presence of corrosion zones (advanced oxidation in the form of ferric oxide), leading to loss of color and major oxidation in the base metal, as shown in (Figure 6) and (Figure 7):

Stiffener steel corrosion at the connection with girder's web. This happened due to advanced oxidation processes. A microscope approach is needed to evaluate the real damage.
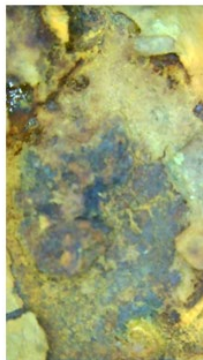
The micrographs show the presence of ferrous oxide and ferric oxide as proof of advance chemical and mechanical mechanisms of damage due to a constant moisture condition.
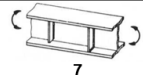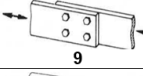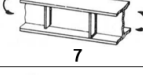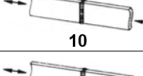
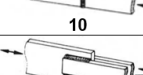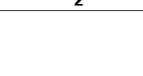***Figure 6.*** *Oxidation and corrosion evidence found on the web stiffener of the main girder element of the Unete steel arch bridge*

ENGLISH VERSION…………………..

Figure 7. *Local buckling of a web stiffener just at the point of a hanger's connection area for the Unete steel arch bridge*

The previous visual inspection determined that said areas govern the remaining fatigue life (the lowest remaining fatigue life). The strength of the material was affected numerically, since having this evidence (of structural and/or chemical irregularities), allows affecting the numerical model locally, using a stress concentration that demands additional (extraordinary) capacity to the structure, making the fatigue life lower than the originally assumed (material in perfect condition). (Table 1) presents the fatigue-affected structural details present in the Unete Bridge, which are similar to the Ang and Munse study. The coefficient of variation associated with each cross-section studied (ΩN) accounted for the variability of the remaining fatigue lives in the numerical calculations, given the numerical approximation of the problem (Munse, 1981).

Table 1. *Structural parameters for the Ang & Munse categories that are directly usable for the structural elements of the Unete steel arch bridge. (Adapted from (Ang and Munse, 1975ª))*

Structural Element	Structural Type Ang & Munse	Description	AASHTO	Log C	m	Ω_N
Main Girder	7	A structural element mainly works in bending with web stiffeners.	C (6)	9.38	2.74	0.70
Secondary Beams.	9	Structural element under axial loading with a shear bolt connection system	B (21)	16.16	7.427	0.70
Transverse Beam.	7	Hot-rolled W-shape structural element, with web stiffeners subjected to alternating flexural stress	C (6)	9.38	2.74	0.70
Arch	10	Butt-welded structural detail for arch hanger element.	B' (8)	9.57	2.880	0.70
Hanger	10	Weldment perpendicular to the axis	E (8)	9.57	2.880	0.70
Arch Relative Bracing System	18	Fillet weldment parallel to an axis	D (9)	8.91	2.67	0.68
Arch Nodal Bracing System	2	Built-up W shape element subjected to flexural stress	B (2)	21.51	9.776	1.13

Since there is already evidence that the primary longitudinal girder of the bridge was exposed to particular moist conditions, generating corrosion already visible in one of the flanges near the area of connection with the web stiffener (See (Figure 6)) and (Table 1) the approximate corrosion adjustment methodology (Adasooriya et al., 2019b) helped in accounting the loss of capacity. This methodology affects the coordinates of the S-N curve in the pristine stage as a function of the exposure of the steel to an aggressive environment. For the case of the Unete Bridge, the environment that best resembles the service conditions is the one that describes the bridge operating in the "presence of water in a natural non-saline state" (adapted from the original methodology).

ENGLISH VERSION……………...

The hardening limit adjustment factors for high and very high cycles are shown in (Table 2).

Table 2. *Endurance limit relations (corroded/sane) for steel conditions*

Endurance limits relations between steels		
Constant Amplitude	$\Delta\sigma_{D,\,corr}/\Delta\sigma_D$	**0.641**
Variable Amplitude	$\Delta\sigma_{L,\,corr}/\Delta\sigma_L$	**0.519**

Where:
$\Delta\sigma D$, corr = endurance limit corroded steel, constant load.
$\Delta\sigma D$ = endurance limit sound steel, constant load.
$\Delta\sigma L$, corr = endurance limit corroded steel, variable load.
$\Delta\sigma L$ = endurance limit sound steel, variable load.

The original curve (with its 4 coordinates), for structural detail No. 7, is adjusted by the relationships indicated above. The stress level corresponding to large cycle fatigue (Nf ≥10,000,00), is affected by 0.519, which is the adjustment factor for long fatigue life-resistant stress (42ksi*0.519 = 21.79ksi). Thus, the coordinates of the new S-N curve (the curve affected by corrosion) are shown in (Table 3).

Table 3. *Original coordinates and affected coordinates of an S-N fatigue curve to account for fatigue effects on the base metal. Adapted from (Adasooriya et al., 2019a)*

$\Delta\sigma i$ (MPa)	$\Delta\sigma i\_corr$ (MPa)	Ni	Log ($\Delta\sigma i$)	Log (Ni)
299	299	10000	2.47519	4.00000
155.0	99.4	100000	1.99719	5.00000
98.0	62.82	500000	1.79808	5.69897
66.0	42.31	2000000	1.6264	6.30103
42.0	21.798	10000000	1.33842	7.00000

The original curve for the structural detail representing the scope area (Category No. 7) and the adjusted curve for corrosion effects are presented in (Figure 8)
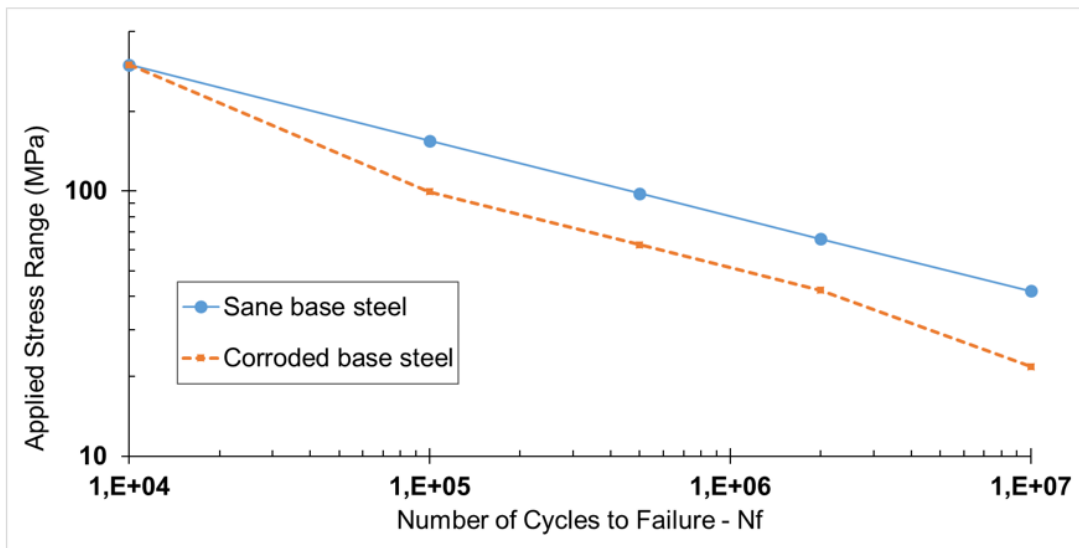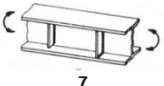

Figure 8. *Fatigue S-N curve for structural detail No 7 (Ang & Munse, 1975), which is affected by corrosion according to the visual inspection and the micrographs available. Corrosion is assumed to happen in a non-salty environment*

The parameters associated with the S-N curve (C and m), and the coefficient of variability (ΩN) are also directly affected to account for the theoretical remaining capacity of the base steel under study when implementing the Weibull model equation in its calculation (See (Table 4)).

37

ENGLISH VERSION……………..…...

Table 4. *(Ang and Munse, 1975) which is closest to the structural member affected by corrosion. Adapted from (Adasooriya et al., 2020)*

Structural Element	Structural Type Ang & Munse	Description	AASHTO	Log C	m	Ω_N
7*	7	Hot-rolled W-shape structural element, with web stiffeners subjected to alternating flexural stress **with corrosion**	B (6)	7.821	2.427	0.875

4.Structural model, load application, and calibration

In parallel to the determination of the fatigue resistance curves for the different elements and structural details, with or without corrosion effects, a numerical model was made to obtain the acting stress ranges for each analysis area by simulation. For this, information on the structural elements such as cross-section, materials, boundary conditions, and general geometry was used. In other words, a model of the bridge was built, to the best extent possible based on the available information. For the current structure, it was possible to develop a model using two-dimensional finite element analyses to account for biaxial distortions. This also involves utilizing elements that have bending stiffness (stiffness to node displacement due to external moment actions), and quadrilateral elements without stiffness in the plane of the quadrilateral, to avoid distortions in the stiffness of the composite section.

The primary aim of this model was to approximate stress histories resulting from the repetitive passage of the fatigue truck, particularly in areas that replicate the connections between elements where structural fatigue phenomena were easily identified during visual inspection. The three-dimensional representation of the model is available in (Figure 9)
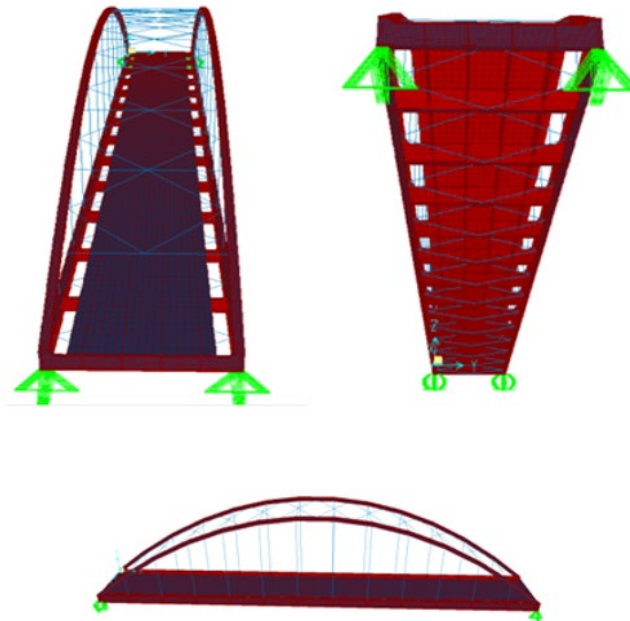

Figure 9. *Finite element model for the structural elements of the Unete steel arch bridge. Hangers, nodal and relative stiffener models used linear frame elements whereas the rest of the structural elements used shell elements*

The development of this model required 83,780 nodes, 2,076 linear elements, and 79,075 area elements which were defined in several thicknesses, helping to simulate the changes in thickness between plates for the various elements that are connected. The area elements also helped to simulate shear connections, generate controlled connections between webs of connected elements, avoid connections between flanges for moment transmission, etc (See (Figure 10). The model has several limitations and simplifications compared to the real bridge structure, but it served as a better complex approach to studying stress concentrations in a coupled state

ENGLISH VERSION………
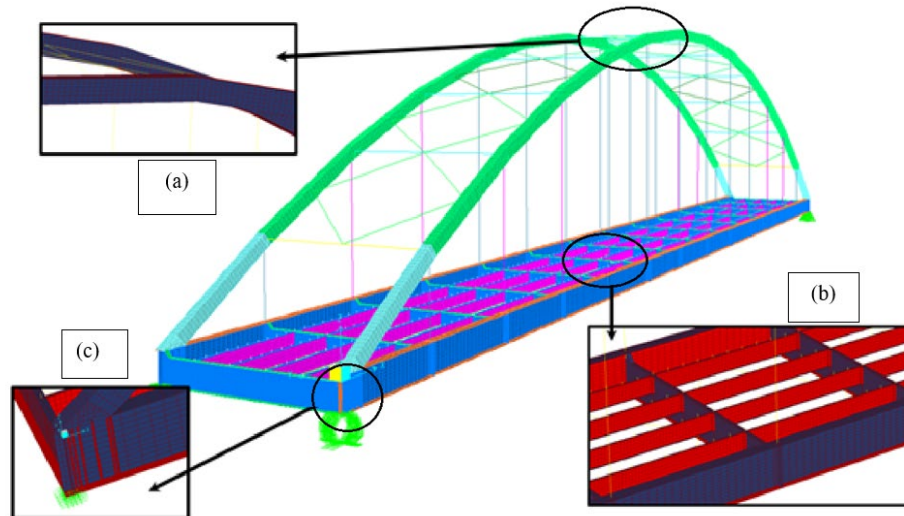
rather than in isolation.

Figure 10. *Finite element shell elements simulating the structural stiffness of a) arch elements, b) slab and hangers, and c) stiffened plate girders*

 For example, for the scope of the present model, the actual geometry of the shear connection's bolts and welding elements were not included. However, it is possible to correctly simulate the beam heights of the larger elements (main girder, transverse beams, longitudinal deck beams), to differentiate web areas, and connection elements such as plates, to differentiate the flange between top and bottom. The hangers continue to be modeled utilizing a bar-type finite element (frame elements).

 To apply the methodology for estimating fatigue vulnerability, loads are simulated by the fatigue truck, and the average daily traffic (ADT) by discriminating the percentage that corresponds to historical heavy traffic. To simulate the variability of traffic on the bridge, the fatigue truck specified in the AASHTO standard was located on the numerical model, following that front axle applies 11.2% and the two rear axles a 44.4% of the reference gross vehicle weight (W) (AASHTO, 2017). The fatigue truck load was affected by an additional 15% to simulate dynamic effects due to the impact on the structure. The truck was represented by the application of punctual loads, approximating the geometry of each axis in the discretized slab. For the case used in this example, a total magnitude of W= 54 kips (240 kN) was used. The axle loads were spaced at distances of 14ft (4.26m) and 30ft (9.14m) and located at the nodes of the mesh that simulated the concrete slab, as close as possible to the required distances. An example of this load placement is shown in (Figure 11).
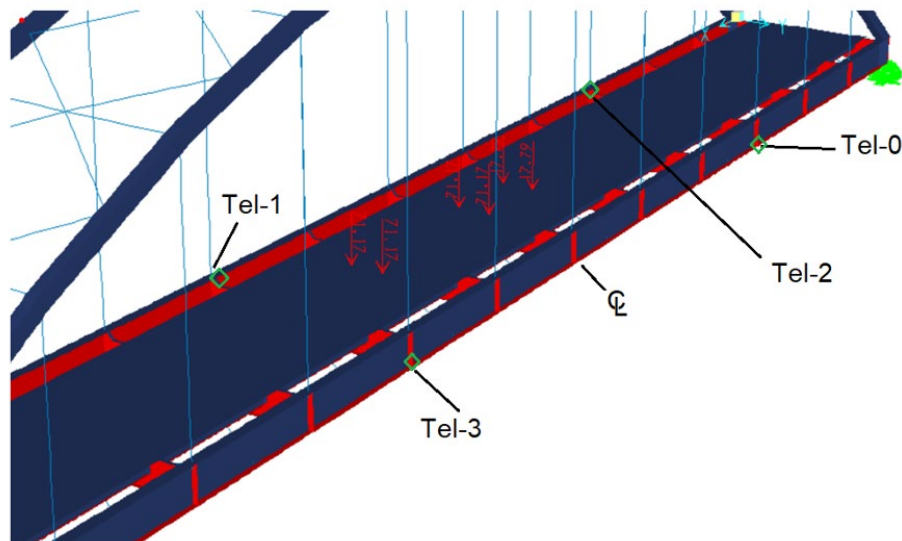

Figure 11. *Simulated truck position along the bridge slab, using simplified punctual loads. Also, localization of telemetry to measure vertical displacements. (Loads in kN)*

The random effects of traffic on the structural elements under study were approximated by the controlled position of the traffic movement, ensuring to generate: i) eccentric states on the bridge, ii) centered steps per lane, and iii) states of total eccentricity for any lane. Five complete steps of the fatigue truck were simulated (entering the bridge and exiting the bridge), for a total of 130 positions in which the truck enters and exits the bridge.

With a structural model ready, the magnitude of the elastic response was verified using a static load test. For the Unete bridge, a load test was performed using trucks of known and controlled weights, measured on a scale close to the area and strategically located on the bridge in compliance with the planned protocol. In this way, it was possible to establish in terms of a controlled deflection, the deformation imposed over the bridge (real reference), to be compared with the theoretical response of the same loads in approximate areas on the structural model. The objective of the calibration was to determine the level of significance achieved by the model to the actual displacement monitored by four (4) telemeters monitoring the lower flanges of the main girder. Thus, the same deflection control points were used in the real and theoretical references. The details of the location of the trucks and the equivalent in the structural model can be seen in (Figure 12).
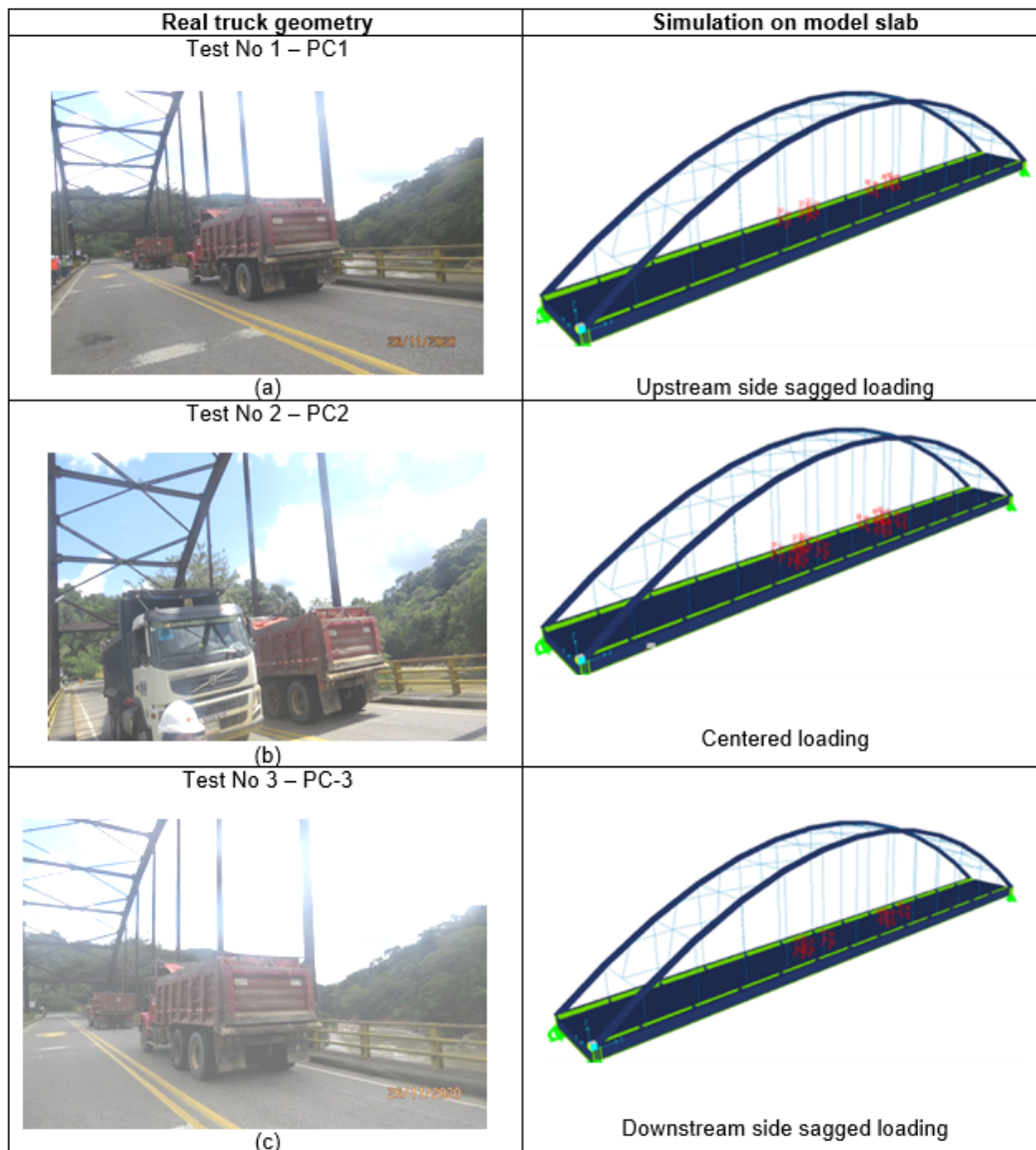

Figure 12. *Truck localization during the load test: a) eccentric load towards the upstream arch, b) centered case of loading, c) eccentric loads towards the downstream arch*

Similar to the fatigue truck, the actual weights of the trucks used during the load test were located in the structural model.

Displacements reported at the node that simulated each rigid connection between each pendulum and the main longitudinal beam of the arch helped in this vertical deflection validation. The graph relating the monitored longitudinal location and the magnitude of the displacement obtained by the model is shown in (Figure 13).
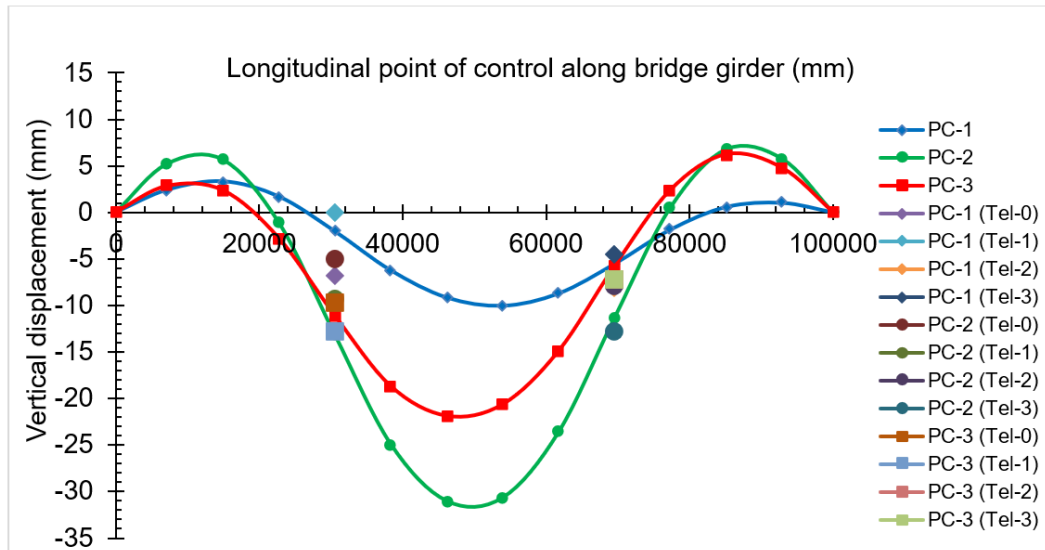

Figure 13. *Vertical displacements along the arch main girder for the Unete steel bridge. This reports the three load tests at the same time*

Thereby, the displacements recorded by the acquisition system in the actual load test were compared with the displacements recorded from the numerical model. The results of the comparison ara available in (Table 5).

Table 5. *Deflection approximation between the finite element model and the reported vertical displacements of the Unete steel arch bridge during the loading tests performed (See (Figure 11.))*

Displacements at controlled points along the girder											
	Δ_REAL (mm)			Δ_SIM (mm)			% Approximation			%Error		
	PC-1	PC-2	PC-3	PC-1	PC-2	PC-3	PC-1	PC-2	PC-3	PC-1	PC-2	PC-3
Point												
Tel-0	-6.8	-5.0	-9.6	-5.05	-10.6	-5.55	-25.7	112.0	-42.2	Low	High	Low
Tel-1	-	-9.4	-12.7	-2.02	-13.14	-11.09	-	39.8	-12.7	High	High	Low
Tel-2	-8.0	-7.8	-7.1	-11.09	-13.14	-2.05	38.6	68.5	-71.1	High	High	Low
Tel-3	-4.5	-12.7	-7.2	-5.55	-10.6	-5.05	23.3	-16.5	-29.9	High	Low	Low

In each of the tests, the best approximation happened in Load Test No. 3 (PC-3), with an 87.3% approximation. In load test PC-2, it was achieved for one of the points at 83.5%, and for load test PC-1, it was achieved up to 76.7%. However, in the PC-2 load test, there are large differences between the Tel-2 and Tel-0 sensors, which may indicate a systematic failure of one of the sensors, since the displacements were small compared to the PC-1 load test, which has less load. In this model calibration stage, the modulus of elasticity was the calibration parameter according to a 3.37% standard deviation that could happen in steels of different grades (Chen et al., 2016). Thus, for a 200GPa (29,000ksi) steel, it is acceptable to use steels with the modulus of elasticity varying in the ranges 193.3GPa ≤ Es ≤ 206.7GPa (28,003ksi ≤ Es ≤ 29,977ksi).

Ten possible values of the modulus of elasticity in the acceptable range (one standard deviation of reference) helped in this parametric study. In this way, results helped in contrasting to the displacements measured on the field, during the load test. The result is shown in (Figure 14), as a cross-function of increasing and decreasing errors. The crossing value happens at a theoretical modulus of elasticity of E=28,960ksi (199.72GPa). For the present investigation, this value was set as the modulus of elasticity that best simulates the model conditions.

ENGLISH VERSION……
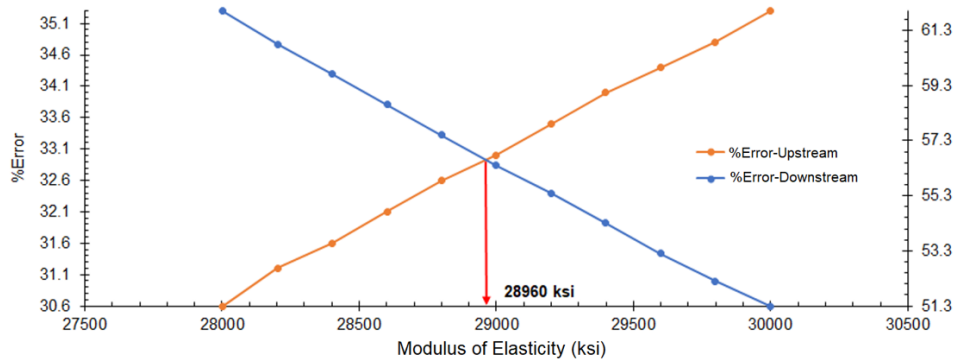

Figure 14. *Systematic variation for the Unete steel bridge modulus of elasticity. Reported errors between the measured point of control vertical displacement and the simulated vertical displacement*

The vertical displacement geometry represented by the calibrated finite element model for the three load tests is shown in (Figure 15), (Figure 16) and (Figure 17)

Figure 15. *Eccentric vertical deformation of the finite element model for the Unete steel arch bridge. Loading case PC-1 (Units in mm)*

Figure 16. *Symmetric vertical deformation of the finite element model for the Unete steel arch bridge. Loading case PC-2 (Units in mm)*
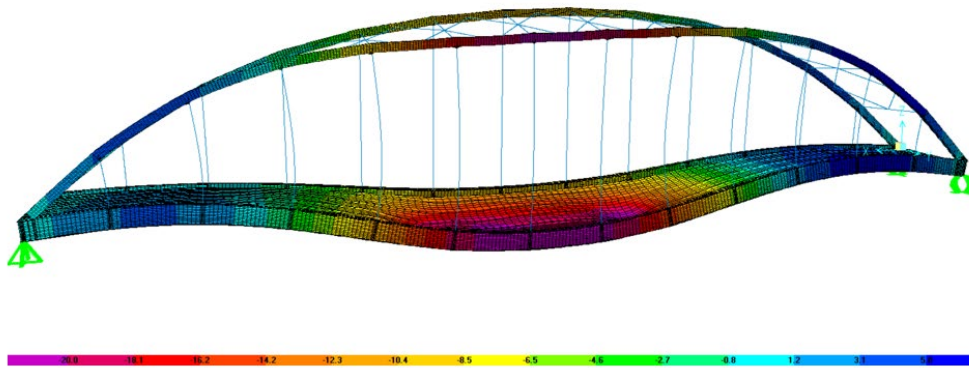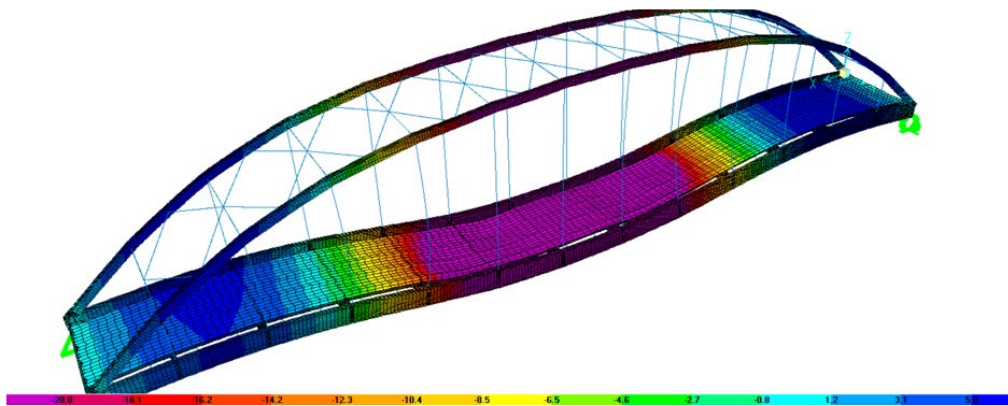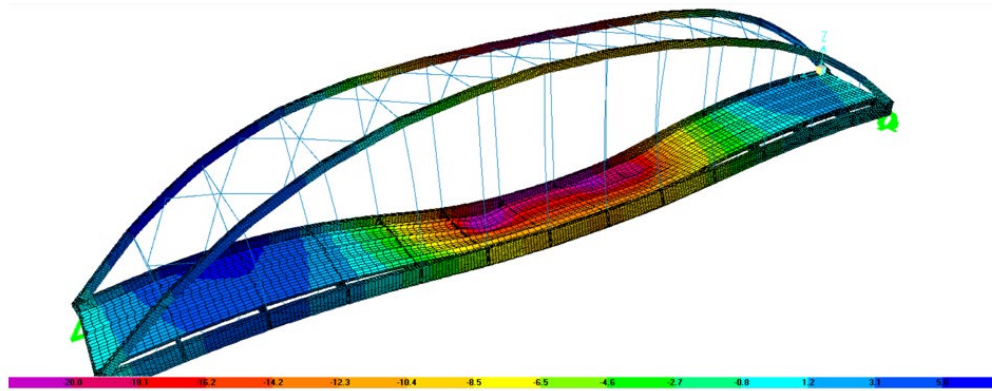
Figure 17. *Eccentric vertical deformation of the finite element model for the Unete steel arch bridge. Loading case PC-3 (Units in mm)*

5. *Estimation of the remaining fatigue life and probability of failure of the structural system*

For the remaining fatigue life, an (see (Equation 1)) was used that considers the distribution factor of trucks per lane -b- which for this bridge is equal to the unit, since each direction has only one lane. The ADT of the road corridor corresponds to 994 vehicles averaged over the last 25 years, with a 47% truck composition. The traffic growth rate -r- was assumed to be 1.5% based on historical traffic behavior. The geometric parameters C and m are those reported in (Table 1) and (Table 4). The modeled finite elements correspond to rectangular shell-type elements, which report stress information at 4 nodes per element. Only the values of one of the flat surfaces helped in generating the stress frequency histograms for the truck positions on the bridge model. (Figure 18) shows the reading zones for each of the elements representing the main longitudinal arch girder for the Unete bridge. Considering that each element is discretized into several elements, only the zone with the highest stress demand was reported, which in this case corresponds to the lower flange.
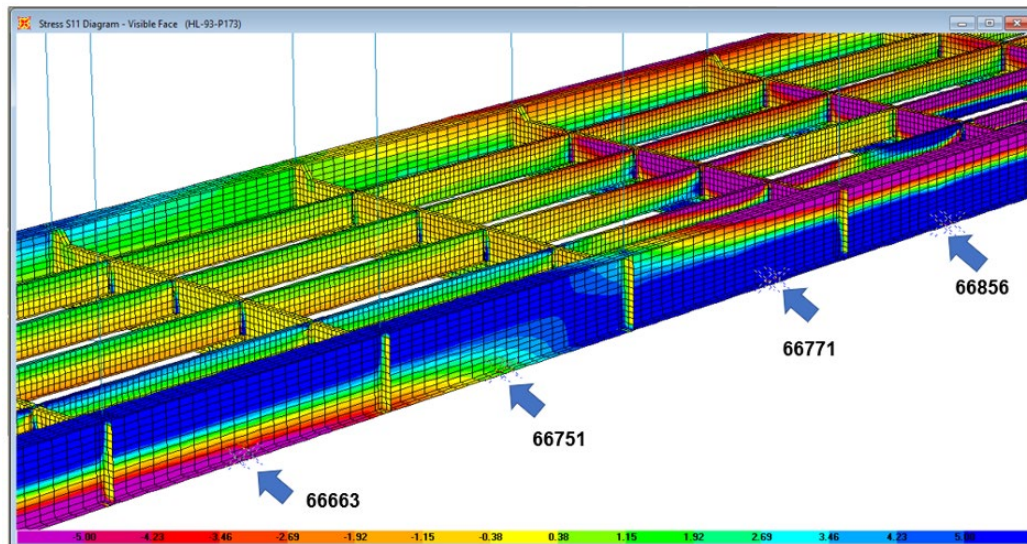
Figure 18. *Shell elements where stresses are the highest in each zone between main deck girders*

The reading of stress concentrations with a more detailed model becomes an important tool for visual inspection activities. This locates important areas of the structure where (theoretically), evidence of fatigue deterioration might be spotted. Therefore, this more complex numerical model also serves as a tool to identify other areas of high-stress concentrations that had not been thought of even with a detailed visual inspection helping to narrow efforts into different areas of the bridge.

ENGLISH VERSION……………………..

Taking the example of element ID # 66751, the stress results of the 130 fatigue truck positions enable the construction of a frequency histogram, where the maximum stress (So), the mean of all the stresses in the mathematical monitoring zone (μrange) and the standard deviation (σrange) were also reported. These values are illustrated in (Figure 19).
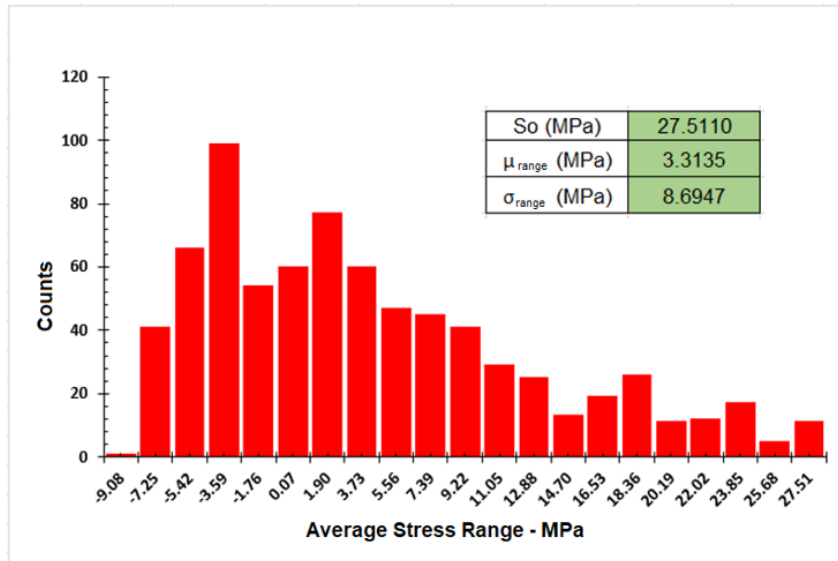

Figure 19. Frequency histogram using 20 ranges for the structural area of a main girder with ID #66751 located near the web-flange joint zone

The equation for the remaining life is based on the complete calculation of the full fatigue life - t - given the traffic conditions (ADT and FT). To determine the parameters of the element being studied, values were substituted into (Equation 1), which is an adapted form of the fatigue remaining life equation originally presented by the Federal Highway Administration (FHWA, 2016).

$$t = \frac{\log \left[\frac{N_T}{b(365 * TPD * F_T)} \right]}{\log (1 + r)}$$

(1)

The parameter *Nt* (see (Equation 2)), which is the number of cycles required for theoretical failure as a function of the stress distribution (obtained for any working zone of any element under study), was constructed following the histogram theory. This is done by obtaining the weighting factor of each stress range studied, based on the total number of numerical monitoring simulations reported. The parameters C and m from (Ang and Munse, 1975) were also required to report *Nt* according to (Equation 2), where n corresponds to the number of stress ranges used to construct the histogram. For the present case, this value is set to 20.

$$N_t = \frac{C}{[\alpha_1 * S_1^m + \alpha_2 * S_2^m + \cdots + \alpha_n * S_n^m]}$$

(2)

Thus, the raw data of the proposed histogram can be detailed in the table below, for a structural element whose values of C and m are 2.3988x109 and 2.74 respectively:

Table 6. Raw data to construct the frequency histogram, for the structural element under study ID#66751, which is located on the web-flange intersection zone for the main girders of Unete steel bridge

#	Range (MPa)	Count	αi	α*Sᵐ
0	-9.08	1	0.00132	0.00
1	-7.25	41	0.05395	0.00
2	-5.42	66	0.08684	0.00
3	-3.59	99	0.13026	0.00
4	-1.76	54	0.07105	0.00
5	0.07	60	0.07895	0.00
6	1.90	77	0.10132	0.59
7	3.73	60	0.07895	2.90
8	5.56	47	0.06184	6.79
9	7.39	45	0.05921	14.19
10	9.22	41	0.05395	23.70
11	11.05	29	0.03816	27.54
12	12.88	25	0.03289	36.13
13	14.70	13	0.01711	27.04
14	16.53	19	0.025	54.49
15	18.36	26	0.03421	99.40
16	20.19	11	0.01447	54.55
17	22.02	12	0.01579	75.48
18	23.85	17	0.02237	133.06
19	25.68	5	0.00658	47.92
20	27.51	11	0.01447	127.30
		760	**1.00**	**731.08**

Therefore, since the sum of the parameters αiSm is 731.08, the magnitude of Nt is

$$N_t = \frac{2.3988 \times 10^9}{731.08} = 3.2812 x 10^6 \ ciclos$$

Having this last parameter allows for (Equation 1) to solve for t, which is the theoretical total fatigue time that the local structural element can resist (in terms of years), from the time the bridge was put into service.

Solving for t, the total theoretical fatigue time is 15.32 years (for the example-design element). If it is considered that the bridge has been in operation for 13 years (t0), then the remaining life will be (see (Equation 3)) 15.32 years - 13 years = 2.32 years. In the present investigation, the remaining life was calculated for each of the structural elements of the bridge.

In this way, it can be indicated that

$$t_{rem} = t - t_0$$

(3)

To estimate the probability of failure, it is necessary to determine the number of cycles to failure (Ncycles, see (Equation 4)) that the bridge has undergone during those last 13 years of operation. For this purpose, a non-linear equation is proposed:

$$N_{cycles} = b(365 * ADT * F_T * F_L) * t * (1 + r)^t$$

(4)

where r is the traffic growth rate, b is the traffic distribution factor per lane, FT, and FL are traffic factors on the bridge lanes and t is the number of years the bridge has been in operation. Thus, replacing the values of the different variables, for this bridge, the approximate number of cumulated fatigue cycles in the last 13 years is:

$$n = N_{cycles} = 0.85 * (365 * 993.9 * 0.47 * 0.85) * 13 years * (1 + 1.5\%)^{13 years} = 1,943,450 \ cycles$$

ENGLISH VERSION………………...

These are fatigue cycles that theoretically the Unete Bridge has accumulated since the day it was put into service, and up to the moment in which this numerical example is made. This parameter is fundamental to be used in the failure probability equation as a

function of the number of cycles applied to date and as a function of the parameters of the structural elements studied in fatigue by Ang and Munse using the Weibull function (Munse, 1981). Thus, parameters q and r and (Equation 6) and (Equation 7) respectivelly are the parameters of the Weibull function (Equation 5) for estimating the probability of failure of a single structural element of the Unete Bridge, in which

$$P_f(n) = 1 - e^{-\left[\left(\frac{n-\varepsilon}{N-\varepsilon}\right)\times\Gamma\left(1+\Omega_N^{1.08}\right)\right]^{\Omega_N^{-1.08}}}$$

(5)

Where N corresponds to the theoretical number of cycles to failure (see (Equation 8)).

$$q = \frac{\frac{s_o*(s_o-\mu_{rango})}{\sigma_{rango}^2} - \left[1+\frac{(s_o-\mu_{rango})}{\mu_{rango}}\right]}{\left[1+\left(\frac{s_o-\mu_{rango}}{\mu_{rango}}\right)\right]^2}$$

(6)

$$r = \frac{s_o-\mu_{rango}}{\mu_{rango}}*q$$ **(7)**

$$N = \frac{C}{S_o^m * \left(\frac{\Gamma(m+q)*\Gamma(q+r)}{\Gamma(q)*\Gamma(m+q+r)}\right)}$$

(8)

As an example, for the calculation of the probability of failure of the element used as example ID#66751, $\Gamma(1+\Omega_N^{1.08})= 0.9051$ *, reporting C as 109.38 = 2.398x109, m=2.74, ΩN=0.70, it is obtained that the probability of failure at the cumulative number of cycles (x = 1,943,450 cycles), then the parameters of the Weibull distribution are:*

$$q = \frac{\frac{27.51\,MPa*(27.51\,MPa-3.313\,MPa)}{(8.695MPa)^2} - \left[1+\frac{(27.51\,MPa-3.313\,MPa)}{3.313\,MPa}\right]}{\left[1+\left(\frac{27.51\,MPa-3.313\,MPa}{3.313\,MPa}\right)\right]^2}$$

$$q = 0.0073$$

$$r = \frac{27.51\,MPa-3.313\,MPa}{3.313\,MPa}*0.0073$$

$$r = 0.0533$$

$$N = \frac{2.398\times10^9}{27.51\,MPa^{2.74}*\left(\frac{\Gamma(2.74+0.0073)*\Gamma(0.0073+0.0533)}{\Gamma(0.0073)*\Gamma(0.1977+0.0073+0.0533)}\right)}$$

$$N = 4.8271\times10^8 ciclos$$

Now when replacing the failure probability equation (see (Equation 5))

ENGLISH VERSION………

$$P_f(n) = 1 - e^{-\left[\left(\frac{1,943,450\ -0}{4.8271\times10^8-0}\right)\times\Gamma\left(1+0.70^{1.08}\right)\right]^{0.70^{-1.08}}}$$

$$P_f(n) = 2.604 \times 10^{-4}$$

This probability of failure numerically indicates the possibility of a complete structural failure of one single element, where the crack manages to generate a complete fracture surface affecting continuity of the cross-section. This is a theoretical state of fatigue.

By repeating this process for all the structural elements that are part of the structural model, summary figures such as (Figure 20) and (Figure 21), report the remaining fatigue life and the probability of failure behavior, for example, for the bridge girders.
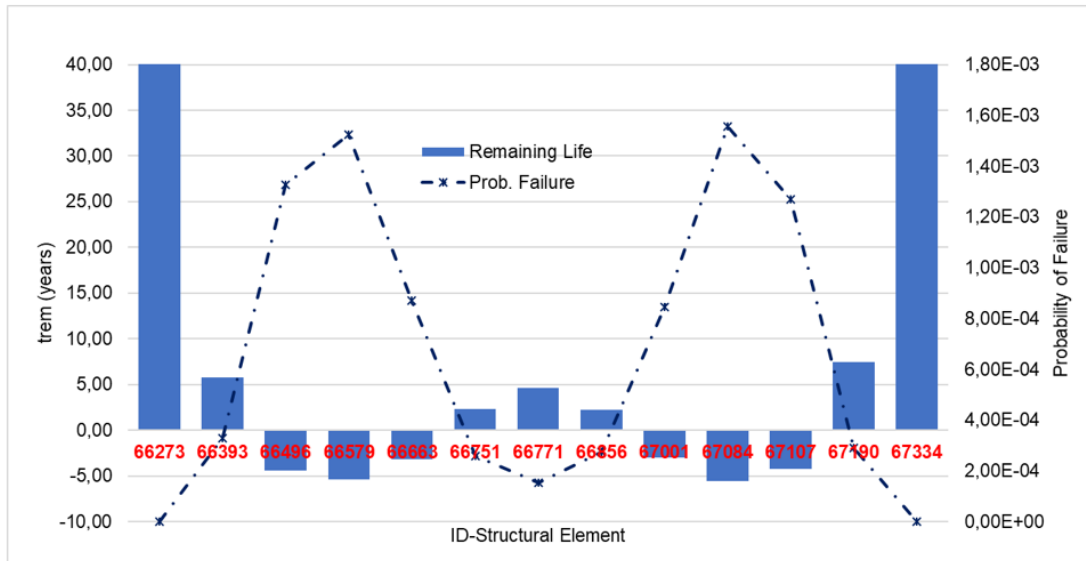

Figure 20. *Main girder structural condition for the downstream arch for the Unete Steel Bridge*
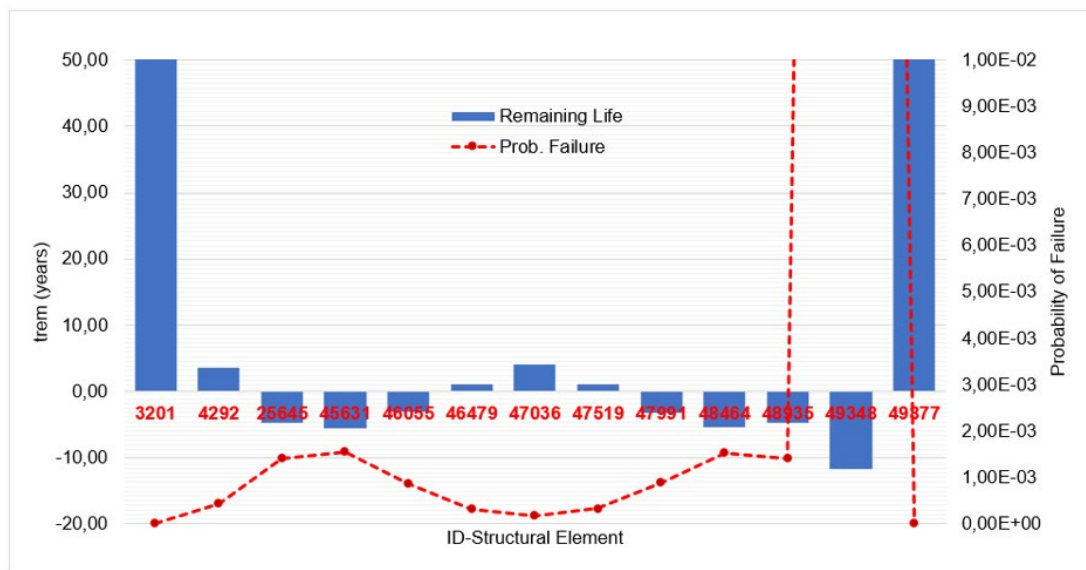

Figure 21. *Main girder structural condition for the upstream arch for the Unete Steel Bridge*

In particular, element ID#49348 (see (Figure 22)), which corresponds to an element of the upstream main girder, was given

47

ENGLISH VERSION………………..

special emphasis in applying the strength modifications (to the S-N fatigue curve) because this element was identified during a primary visual inspection as having oxidation and corrosion conditions as shown in (Figure 6) and (Figure 7). To account for the effect of corrosion, the effect on the structural category parameters was modeled, as shown in (Table 4). The probabilities of bridge failure are now governed by the loss of capacity in this structural element.
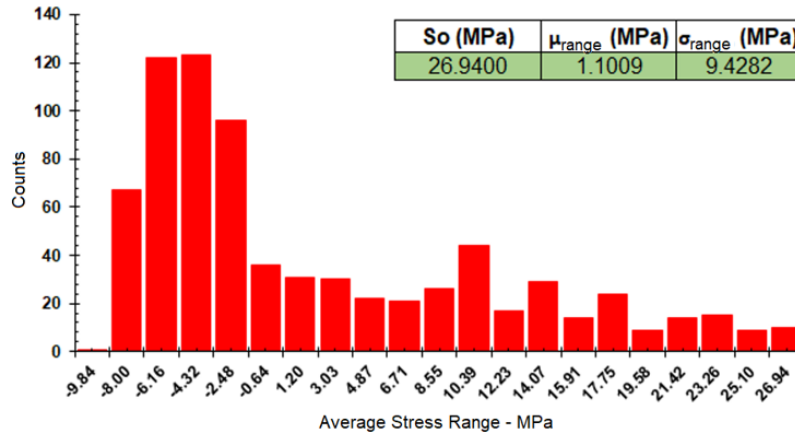

Figure 22. *Frequency histogram using 20 ranges for the structural area of a main girder with ID #49348 located at the web-flange joint zone with evidence of advanced corrosion*

6. Probability of system failure under a simplified progressive collapse model

To find the system probability of failure (the whole structure), a basic probabilistic model is proposed, which considers the probability of failure of each element and proposes a cumulative failure scenario by the number of elements and their corresponding cumulative collapse probability. The probabilistic model, as indicated above, is approximate and does not account for the conditional probabilities of cumulative failure. In other words, it assumes that fatigue failure is mutually exclusive and yet cumulative. For the case at hand, (Equation 9) should be applied for the calculation of the probability affected by the redundancy factor (γ, assumed 1.0 for the present investigation) and the product of probabilities.

$$P(E_{TF}) = 1 - \prod_{i=1}^{n}(1 - \gamma_i * P(E_i))$$

(9)

With these data, a cumulative probability graph (fatigue vulnerability curve) is constructed by applying the damage accumulation equation (Equation 9). The results indicate that the failure probabilities of the main longitudinal girders correspond to 84% of the complete failure probability of the bridge (See (Figure 23)), which indicates that the bridge decking system is the most important area for fatigue prevention and control in the bridge. Thus, the theoretical curve of the probability of failure of the entire bridge was constructed as a function of the number of fatigued elements (in this case, all the modeled elements).
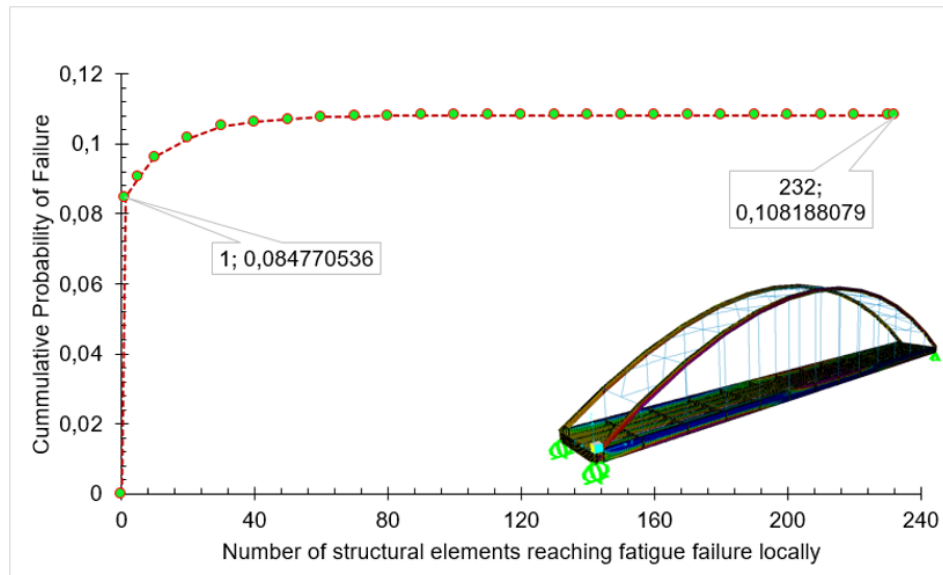
ENGLISH VERSION………………..

Figure 23. *The theoretical probability of failure curve (fatigue vulnerability curve) for the Unete steel arch bridge as a function of the joint state of structural elements meeting fatigue failure*

7. Discussion and conclusions

The first element of this curve (see (Figure 23)), corresponds to the lowest fatigue capacity of all structural members, which is the candidate for detailed field review, corresponding to the main girder, where corrosion phenomena are taking place. This is evident since the steel that is affected by oxidation/corrosion effects does not have the same mechanical capacities as a healthy steel and this is represented both in lower magnitudes of yield stress and ultimate stress, as well as in fatigue resistance.

The asymptotic behavior of the cumulative probability curve indicates that the maximum theoretical probability of fatigue failure of the structure is far from 1.0, presenting a safe state of the bridge operation (Pf<0.50). However, this does not exclude the bridge from a continuous observation in service condition due to the overly complex nature of steel fatigue.

In conclusion, the lowest available remaining life of the entire structure corresponds to -11.68 years corresponding to the area affected by oxidation (low corrosion) of the main longitudinal girder of the bridge with a probability magnitude of 8.477×10^{-2}. This is mainly due to the aggressive effect of corrosion on the structural element. The theoretical cumulative probability of failure of the entire structure is 1.08188×10^{-1}, which can be interpreted as "low fatigue". However, visual inspections are always recommended to be able to observe local damage and actual damage to the structure, which may appear without warning.

In conclusion, the proposed methodology, despite being a numerical approximation derived from field activities, offers an economically feasible approach with a satisfactory level of reliability in assessing fatigue vulnerabilities of a complex structure subjected to fluctuating loads. This approach allows the structural evaluator or investigator to estimate the remaining fatigue life of primary structural elements (main elements), as well as select connecting and secondary elements. These estimates are based on recommended field pathology and material investigation in the structure.

8. Acknowledgments

ENGLISH VERSION………………...

9. References

AASHTO. (2017). *AASHTO LRFD Bridge Design Specifications, 8th Edition.*

Adasooriya, N. D.; Hemmingsen, T.; Pavlou, D. (2020). *S-N curve for riveted details in corrosive environment and its application to a bridge. Fatigue and Fracture of Engineering Materials and Structures, December 2019, 1–15. https://doi.org/10.1111/ffe.13193*

Adasooriya, N. D.; Pavlou, D.; Hemmingsen, T. (2019a). *Fatigue strength degradation of corroded structural details: A formula for S-N curve. Fatigue and Fracture of Engineering Materials and Structures, September, 1–13. https://doi.org/10.1111/ffe.13156*

Adasooriya, N. D.; Pavlou, D.; Hemmingsen, T. (2019b). *Fatigue strength degradation of corroded structural details: A formula for S-N curve. Fatigue and Fracture of Engineering Materials and Structures, September, 1–13. https://doi.org/10.1111/ffe.13156*

Ang, A. H.-S.; Munse, W. H. (1975). *Practical Reliability Basis for Structural Fatigue. National Structural Engineering Conference - ASCE, 14–18.*

Chen, Z.; Gandhi, U.; Lee, J.; Wagoner, R. H. (2016). *Variation and consistency of Young's modulus in steel. Journal of Materials Processing Technology, 227, 227–243. https://doi.org/10.1016/j.jmatprotec.2015.08.024*

FHWA, F. H. A.-. (2013). *Manual for Repair and Retrofit of Fatigue Cracks in Steel Bridges.*

FHWA, F. H. A.-. (2016). *Design and Evaluation of Steel Bridges for Fatigue and Fracture. http://www.nhi.fhwa.dot.gov/training/nhistore.aspx*

JTG-D64. (2015). *Especificaciones generales de diseño para puentes de acero para autopistas. Ministerio de Transporte de la República Popular de China.*

Munse, W. H. (1981). *Fatigue Criteria for Ship Structure Details. Equation 15.*